PAPER • OPEN ACCESS

Interaction-motif-based classification of self-organizing metabolic cycles

To cite this article: Vincent Ouazan-Reboul *et al* 2023 *New J. Phys.* **25** 103013

View the article online for updates and enhancements.

New Journal of Physics

The open access journal at the forefront of physics

PAPER

Interaction-motif-based classification of self-organizing metabolic cycles

Vincent Ouazan-Reboul[1] ⬤, Ramin Golestanian[1,2,*] ⬤ and Jaime Agudo-Canalejo[1,*] ⬤

[1] Max Planck-Institute for Dynamics and Self-Organization, Am Fassberg 17, D-37077 Göttingen, Germany
[2] Rudolf Peierls Centre for Theoretical Physics, University of Oxford, OX1 3PU Oxford, United Kingdom
* Authors to whom any correspondence should be addressed.

E-mail: ramin.golestanian@ds.mpg.de and jaime.agudo@ds.mpg.de

Abstract

Particles that are catalytically-active and chemotactic can interact through the concentration fields upon which they act, which in turn may lead to wide-scale spatial self-organization. When these active particles interact through several fields, these interactions gain an additional structure, which can result in new forms of collective behavior. Here, we study a mixture of active species which catalyze the conversion of a substrate chemical into a product chemical, and chemotax in concentration gradients of both substrate and product. Such species develop non-reciprocal, specific interactions that we coarse-grain into attractive and repulsive, which can lead to a potentially complex interaction network. We consider the particular case of a metabolic cycle of three species, each of which interacts with itself and both other species in the cycle. We find that the stability of a cycle of species that only chemotax in gradients of their substrate is piloted by a set of two parameter-free conditions, which we use to classify the low number of corresponding interaction networks. In the more general case of substrate- and product-chemotactic species, we can derive a set of two high-dimensional stability conditions, which can be used to classify the stability of all the possible interaction networks based on the self- and pair-interaction motifs they contain. The classification scheme that we introduce can help guide future studies on the dynamics of complex interaction networks and explorations of the corresponding large parameter spaces in such metabolically active complex systems.

1. Introduction

Chemotactic particles, which develop force-free motion in response to gradients, have been shown to develop effective interactions through the fields upon which they act, independently of the particular mechanism through which they move [1]. Such interactions have for instance been observed in diffusiophoretic [2–4] and thermophoretic [5–7] colloids, as well as for chemotactic microorganisms [8, 9]. Field-mediated active interactions have the particularity of being nonreciprocal, meaning that the response of a particle A to the presence of another particle B is different from the response of B to A [10–13]. This feature can lead to new forms of collective behavior as compared to reciprocally-interacting systems [14, 15]. For example, binary mixtures of catalytically active particles may spontaneously form self-propelled clusters [16]. The models describing active phoretic particles can be extended to the case in which particles act upon and interact through several chemical fields, which introduces a nontrivial topology to the network of interactions among different particle species. This interaction topology can allow the self-organization of a mixture of self-repelling species [17], which is not possible for simpler interaction schemes, and can lead to super-exponential aggregation of complementary catalysts, which could have been relevant in the emergence of living matter [18].

    Taking into account the presence of several chemical fields leads to an explosion in the number of possible interaction patterns that active phoretic species can develop, which in turn makes the determination of the conditions in which mixtures of such species can self-organize rather challenging. To overcome this

issue, inspiration can be found from the methods used for tackling the protein folding problem, which consists in understanding and characterizing the process through which an initially linear chain of amino acids folds into a dense three-dimensional structure [19], and determining which structure a given sequence folds into. One of the challenges that is encountered in this setting is that proteins are composed of 20 possible amino acid species, leading to a number of possible sequences going as 20^n for a chain of n amino acids, thus making the enumeration of biologically-relevant chains of hundreds of amino acids combinatorially complex. In order to decrease this number, one approach is to coarse-grain the amino acids into a smaller number of categories that have simple interaction rules. This is the basis of the celebrated HP lattice model [20, 21], which considers two categories of hydrophobic and polar amino acids, although it has also been extended to larger alphabets [22–24]. While current state of the art methods can leverage abundant computational power and large data sets, which allows for accurate predictions of the structure of biological proteins [25], simple lattice models have impressive predictive power [26, 27], with the hydrophobic or polar nature of the residues having been shown to have a strong influence on protein structure independently of their particular nature [28]. Moreover, simple proteins having been successfully designed based on the binary alphabet used in the HP model [29].

In this work, we use a similar approach to determine the ability of catalytic species involved in small metabolic cycles to self-organize, coarse-graining their interactions into attractive 'A' or repulsive 'R' but with the important new element of non-reciprocity. We are able to systematically classify the (linear) stability of homogeneous mixtures of catalytic particles participating in metabolic cycles, and thus their tendency to spatially self-organize, based on which interaction motifs they contain. We stress that our focus here is on determining if there is an emergent *spatial* organization of the catalysts, and not on the kinetic properties of the total catalytic flux of the cycle. The latter can be studied in detail for cycles and networks of arbitrary complexity, assuming a well-mixed system without spatial structure, using the methods of metabolic flux analysis [30], flux balance analysis [31], metabolic control analysis [32], or by direct solution of the reaction mass balance equations [33]. Our article is structured as follows. Section 2 describes the basic framework and summarizes the classification of the metabolic networks. Section 3 describes the model in detail, and our method for analyzing the stability of metabolic cycles. In section 4, we classify the stability of cycles composed of species with a single chemotactic coefficient corresponding to the substrate of the reaction they catalyze, which can be done using a simple, parameter-free instability criterion. Finally, in section 5 we generalize this classification to species that are chemotactic to both their substrate and their product, by deriving two instability criteria and determining which interaction motifs need to be present for these instability conditions to be satisfied. Section 6 contains some discussions while some of the details of the calculations are relegated to the appendices.

2. Model overview and summary of results

We study self-organization of catalytically active particles belonging to M distinct species, and K chemical fields upon which these particles act. In particular, each particle of species m converts a substrate chemical, with index $k = \text{s}(m)$, into a product chemical $k' = \text{p}(m)$ at a rate α_m (figure 1(a)). The functions $\text{s}(m)$ and $\text{p}(m)$ therefore map each catalytic species index to the index of the substrate and product chemical, respectively, and define the topology of the *catalytic network*. Assuming that catalysts of species m have a concentration ρ_m, we can then write the evolution equations for the concentrations of the K chemical fields they produce and consume as:

$$\partial_t c_k(\mathbf{r}, t) = D^{(k)} \boldsymbol{\nabla}^2 c_k + \sum_m \left(\delta_{k,\text{p}(m)} - \delta_{k,\text{s}(m)} \right) \alpha_m \rho_m, \tag{1}$$

where $D^{(k)}$ is the diffusion coefficient of chemical species k, and $\delta_{m,n}$ is the Kronecker symbol, verifying $\delta_{m,n} = 1$ if $m = n$ and 0 else.

The active particles we consider are also taken to be chemotactic for both their substrate and their product. In a concentration gradient of its substrate $\nabla c_{\text{s}(m)}$, a particle of species m develops a velocity going as $-\mu_m^{(\text{s})} \nabla c_{\text{s}(m)}$, which takes it towards the high (respectively low) concentrations of its substrate if $\mu_m^{(\text{s})}$ is negative (respectively positive). The same is true for gradients of the product of species m, to which a product mobility $\mu_m^{(\text{p})}$, also of arbitrary sign, and independent from $\mu_m^{(\text{s})}$, is associated. We can then write the following continuity equation for the concentrations of the active species ρ_m:

$$\partial_t \rho_m(\mathbf{r}, t) = \boldsymbol{\nabla} \cdot \left[D_{\text{p}} \boldsymbol{\nabla} \rho_m + \left(\mu_m^{(\text{s})} \boldsymbol{\nabla} c_{\text{s}(m)} + \mu_m^{(\text{p})} \boldsymbol{\nabla} c_{\text{p}(m)} \right) \rho_m \right], \tag{2}$$

where we take all catalysts to have the same diffusion coefficient D_{p}.
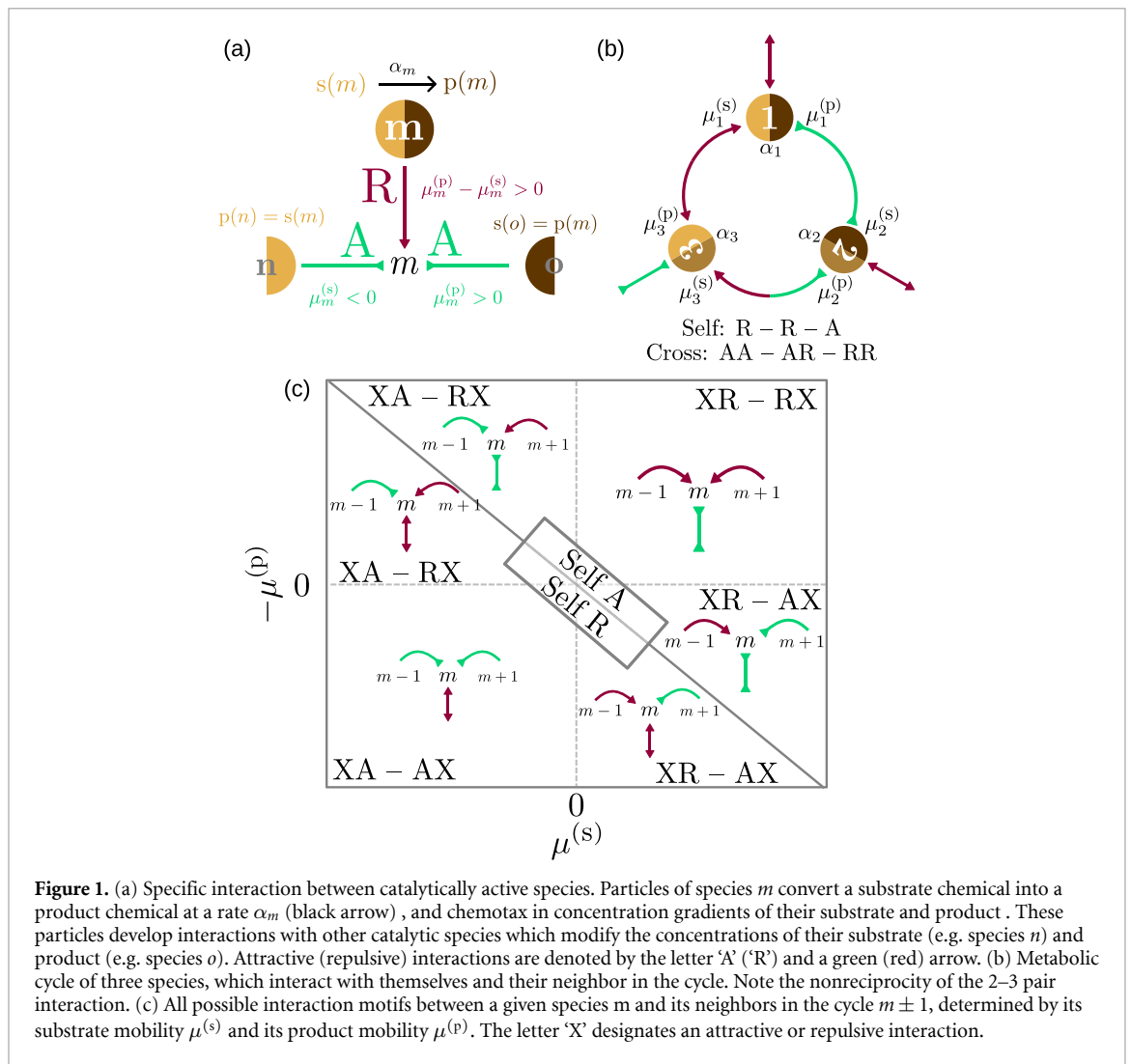
Figure 1. (a) Specific interaction between catalytically active species. Particles of species m convert a substrate chemical into a product chemical at a rate α_m (black arrow) , and chemotax in concentration gradients of their substrate and product . These particles develop interactions with other catalytic species which modify the concentrations of their substrate (e.g. species n) and product (e.g. species o). Attractive (repulsive) interactions are denoted by the letter 'A' ('R') and a green (red) arrow. (b) Metabolic cycle of three species, which interact with themselves and their neighbor in the cycle. Note the nonreciprocity of the 2–3 pair interaction. (c) All possible interaction motifs between a given species m and its neighbors in the cycle $m \pm 1$, determined by its substrate mobility $\mu^{(s)}$ and its product mobility $\mu^{(p)}$. The letter 'X' designates an attractive or repulsive interaction.

From equations (1) and (2), it can be deduced that the catalytic species develop interactions mediated by the concentration fields of their respective substrates and products: through their chemotactic mobilities, the active particles we consider are able to develop induced velocities in response to chemical gradients created by the catalytic activity of other particles. Effective interactions relying on this mechanism have been previously shown to lead to self-organization of catalytic mixtures [16–18, 34]. Here, because we study species which act upon and react to a restricted subset of concentration fields, the emergent interactions are specific: a given species m only responds to concentration gradients of its substrates and products, and thus only species which act on these particular concentration fields will elicit a induced response in m (figure 1(a)). Moreover, these interactions are nonreciprocal: in general, the velocity response of species m to species n is different from the response of n to m (figure 1(b)). Based on the choice of its mobilities, each catalyst species then develops a specific pattern of induced velocities to the other catalytic species, which determines the *interaction network* among species.

In this work, we seek to understand how different combinations of interaction patterns can lead to self-organization of catalytic mixtures whose components interact according to a network of specific, nonreciprocal interactions. We focus our study on the particular case of three species which are arranged into a model metabolic cycle (figure 1(b)), in which the substrate of species 1 is the product of species 3 and its product is the substrate of species 2, whose product is in turn the substrate of species 3. Catalytic species involved in such a cycle develop interactions with both other species and themselves, according to a set of six patterns shown in figure 1(c). In the later sections, we will systematically study the stability of all interaction pattern combinations, and find that any metabolic cycle of three species can be mapped onto nine 'elementary' sets of networks, each of which belongs to one of five stability classes. The stability of all elementary network sets is listed in table 1, with the possible stability classes comprising the following cases:

Table 1. classification of the different emergent possibilities for a size-3 metabolic cycle. Left column: instability class; see main text for the definitions. Middle-left column: single-species interaction motifs, with A denoting self-attracting species and R denoting self-repelling species. X can correspond to any sense of interaction. Middle-right column: pair interaction motifs. Right column: corresponding metabolic cycle. Dark blue motifs are always destabilizing, and light blue motifs promote instability if some inequality on the mobilities of the involved species is verified (see table 2).

Stability class	Interaction motifs		Elementary cycle
	Self [11–22–33]	Mutual [12–23–31]	
Always unstable	A—A—A	XX—XX—XX	
Type-I unstable	R—A—X	XX—XX—XX	
Type-IIa (strongly) unstable	R—R—R	AR—AA—RR	
	R—R—R	AR—AA—RA	
	R—R—R	AA—AA—RR	
Type-IIb (weakly) unstable	R—R—R	AA—RA—RA	
	R—R—R	RA—AA—AA	
Stable	R—R—R	AA—AA—AA	
	R—R—R	AR—AR—AR	

- Always unstable: cycles of three self-attracting species which self-organize no matter the choice of parameters.
- Type-I unstable: cycles which involve self-attracting species, and which can self-organize if self-attraction overcomes self-repulsion.
- Type-IIa (or strongly) unstable: cycles of self-repelling species involving at least one instability-favoring pair.
- Type-IIb (or weakly) unstable: cycles of self-repelling species which include at least one pair which can be instability-favoring if some constraint on the mobilities of the active species is satisfied.
- Always stable: cycles of self-repelling species which do not include instability-favoring pair motifs, and cannot self-organize.

3. Model description

We consider a set of $M = 3$ catalytic species involved in a metabolic cycle as described in the previous section. Due to this cycle structure, there are $K = 3$ chemical fields through which the catalysts interact, and we choose the convention that the substrate of catalytic species m, which is also the product of species $m - 1$, is indexed as $s(m) = p(m - 1) = m$. Note that, throughout this work, we will use periodic indices, so that species 0 is species 3 and species 4 corresponds to species 1, and so on.

In this setting, we perform a linear stability analysis on equations (1) and (2) (see appendix A) and find that the stability of the cycle is set by the eigenvalue equation

$$\lambda \delta \rho_m = -\sum_{n=1}^{3} \Lambda_{m,n} \delta \rho_n, \tag{3}$$

with $\delta \rho_n$ being the perturbation of the concentration of species n. The catalytic species involved in the metabolic cycle then undergo spatial self-organization through a system-wide instability if $\text{Re}(\lambda) > 0$, the conditions for which we seek to uncover in the rest of this work. Equation (3) involves $\boldsymbol{\Lambda}$, which is the matrix of effective interactions between the active species, and has coefficients

$$\Lambda_{m,n} = \begin{cases} \alpha_{m-1} \tilde{\mu}_m^{(s)} \rho_{0m} & \text{if } n = m - 1, \\ \alpha_m \left(\tilde{\mu}_m^{(p)} - \tilde{\mu}_m^{(s)} \right) \rho_{0m} & \text{if } n = m, \\ -\alpha_{m+1} \tilde{\mu}_m^{(p)} \rho_{0m} m & \text{if } n = m + 1. \end{cases} \tag{4}$$

Here, we have set $\tilde{\mu}_m^{(s)} = \mu_m^{(s)}/D^{(m)}$ and $\tilde{\mu}_m^{(p)} = \mu_m^{(p)}/D^{(m+1)}$, and ρ_{0m} is the density of species m in the homogeneous state. The response of species m to species n is attractive if $\Lambda_{m,n} < 0$, and repulsive if $\Lambda_{m,n} > 0$. We can then characterize the structure of the interactions of a metabolic cycle via the signs of the self- and pair-interactions of its constituent species, the encoding of which is shown in figure 1(b): a repulsive interaction is denoted by the letter 'R', and an attractive interaction by the letter 'A'. In the example of figure 1(b), the self-interaction pattern is written as R–R–A, meaning that species 1 and 2 are self-attracting, and species 3 is self-repelling. The pair interactions, meanwhile, read AA–AR–RR, which denotes the fact that species 1 and 2 attract each other, species 2 chases species 3, and species 1 and 3 both repel each other.

According to equation (4), the self-interaction of a given species m can be expressed as a linear combination of its cross-interactions with other species. This constrains the signs of the triplet $(\Lambda_{m-1,m}, \Lambda_{m,m}, \Lambda_{m,m+1})$ to belong to one of the six, rather than the theoretically possible $2^3 = 8$, patterns shown in figure 1(c). Any possible interaction network for a metabolic cycle of three species can then be built by independently choosing one of these six patterns for each species. In the rest of this work, we classify the stability behavior of all such possible $6^3 = 216$ networks.

4. Phase diagram for product-insensitive species

The number of possible interaction combinations can be reduced by setting the product mobilities of all species to zero, i.e. $\mu_m^{(p)} = 0$, which sets $\Lambda_{m,m+1} = 0$ for all species. This assumption is also consistent with experimental data, as enzyme chemotaxis has so far only been studied in the presence of substrate concentration gradients [35–38]. In this case, catalysts of a given species m can only interact with catalysts of the same species or the previous species $m - 1$. Additionally, the self-interaction now satisfies $\Lambda_{m,m} = -\frac{\alpha_m}{\alpha_{m+1}} \Lambda_{m,m-1}$, meaning that the self-interaction of a given species is of the opposite sign as its response to the previous species. Only two interaction motifs are then possible in this case, one being self-attracting and repelled by the previous species, and the other, self-repelling and attracted by the previous species. This makes for a total number of possible interaction networks of $2^3 = 8$, which are easily enumerated.

We can determine the stability of each network of purely substrate-sensitive interactions by carrying out the linear stability analysis, which in this particular case yields parameter-independent instability conditions, and determining how these conditions intersect with regions of the parameter space corresponding to the different interaction patterns. The eigenvalues for strictly substrate-sensitive species are found as

$$\lambda_\pm = |\Lambda_{1,1}| \left[-\frac{1}{2} \left(\tilde\Lambda_1 + \tilde\Lambda_2 + \tilde\Lambda_3 \right) \pm \frac{1}{2} \sqrt{ \left(\tilde\Lambda_1 + \tilde\Lambda_2 + \tilde\Lambda_3 \right)^2 - 4 \left(\tilde\Lambda_1 \tilde\Lambda_2 + \tilde\Lambda_2 \tilde\Lambda_3 + \tilde\Lambda_1 \tilde\Lambda_3 \right) } \right]. \tag{5}$$

Here, we have normalized the self-interactions with $\Lambda_{1,1}$, such that $\tilde\Lambda_m = \frac{\Lambda_{m,m}}{|\Lambda_{1,1}|}$ is the ratio of the self-interaction of species m to the magnitude of the self-interaction of species 1. From equation (5), two instability conditions can be deduced, which we respectively name type-I and type-II:

$$\text{type-I:} \quad \tilde\Lambda_1 + \tilde\Lambda_2 + \tilde\Lambda_3 < 0, \tag{6}$$

and

$$\text{type-II:} \quad \begin{cases} \tilde\Lambda_1 + \tilde\Lambda_2 + \tilde\Lambda_3 > 0, \\ \tilde\Lambda_1 \tilde\Lambda_2 + \tilde\Lambda_2 \tilde\Lambda_3 + \tilde\Lambda_1 \tilde\Lambda_3 < 0. \end{cases} \tag{7}$$

The type-I condition equation (6) only contains self-interaction terms, and corresponds to having a mixture that is self-attracting on average, as found in [16, 34] for systems with a non-cyclic interaction topology. In contrast, the type-II condition equation (7) includes terms involving pairs of particle species. This condition allows for the mixture to be self-repelling on average, and instead requires pairs with opposite self-interaction signs to have stronger self-interaction than pairs with equal self-interaction signs.

We can then study separately the cases where species 1 is self-attracting ($\tilde\Lambda_1 = -1$) and self-repelling ($\tilde\Lambda_1 = 1$). In the case of a self-attracting species 1, $\tilde\Lambda_1 = -1$, we rewrite equations (6) and (7) as inequalities of $\tilde\Lambda_3$ as a function of $\tilde\Lambda_2$. It can be shown that, if $\tilde\Lambda_2 < 1$, the first and second order conditions are complementary, so that at least one is always satisfied, and that the overall instability condition then writes:

$$\begin{cases} \tilde\Lambda_2 \geqslant 1, \\ \tilde\Lambda_3 < \dfrac{\tilde\Lambda_2}{\tilde\Lambda_2 - 1}, \end{cases} \text{or } \tilde\Lambda_2 < 1. \tag{8}$$

Furthermore, we can also write an oscillation condition by determining which parameters make equation (5) complex with a positive real part. Parameters which make the term under the square root in equation (5) also satisfy the type-I instability condition, leading to the oscillation condition

$$\begin{cases} \tilde\Lambda_2 < 0, \\ \tilde\Lambda_3 \in \left[-\left(1 + \sqrt{-\tilde\Lambda_2} \right)^2, -\left(1 - \sqrt{-\tilde\Lambda_2} \right)^2 \right]. \end{cases} \tag{9}$$

We plot the corresponding stability phase diagram in $(\tilde\Lambda_2, \tilde\Lambda_3)$ coordinates in the left panel of figure 2, and find that cycles of purely substrate-sensitive species are always unstable if they contain two or three self-attracting species, while they can be either stable or unstable if they contain one self-attracting and one self-repelling species. The oscillation condition equation (9), meanwhile, is only compatible with cycles of three self-attracting species (figure 2, purple region). These predicted stability diagram was confirmed by particle-based Brownian dynamics simulations (see appendix B). In figure 2, filled circles correspond to simulations that remained homogeneous, while empty circles correspond to simulations that displayed clustering. Oscillations were never observed in simulations, which we ascribe to the fact that the real part of the complex eigenvalue is always larger than its imaginary part, meaning that the system is out of the linear-perturbation regime by the time a full oscillation period is completed.

We now consider species 1 to be self-repelling, $\tilde\Lambda_1 = 1$. Using similar calculations as in the self-attracting case, we find the instability condition

$$\begin{cases} \tilde\Lambda_2 \geqslant -1, \\ \tilde\Lambda_3 < -\dfrac{\tilde\Lambda_2}{\tilde\Lambda_2 + 1}, \end{cases} \text{or } \tilde\Lambda_2 < -1. \tag{10}$$

Plotting the corresponding phase diagram in the right panel of figure 2, we once again find that cycles of two self-attracting, product-insensitive species are always unstable and that cycles including only one
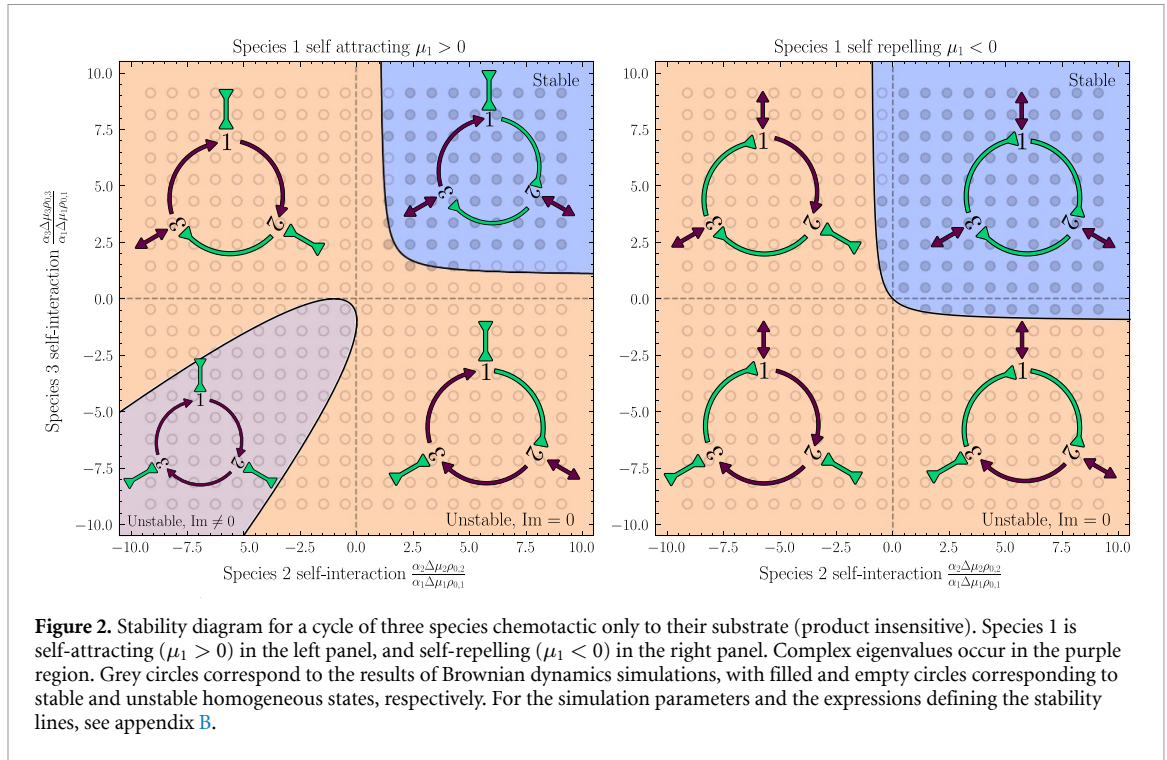
Figure 2. Stability diagram for a cycle of three species chemotactic only to their substrate (product insensitive). Species 1 is self-attracting ($\mu_1 > 0$) in the left panel, and self-repelling ($\mu_1 < 0$) in the right panel. Complex eigenvalues occur in the purple region. Grey circles correspond to the results of Brownian dynamics simulations, with filled and empty circles corresponding to stable and unstable homogeneous states, respectively. For the simulation parameters and the expressions defining the stability lines, see appendix B.

self-attracting species can either be stable or unstable. Finally, we find that a cycle composed of three self-repelling species verifying $\mu^{(\mathrm{p})} = 0$ is always stable. The oscillation condition obtained with $\tilde{\Lambda}_1 = 1$ is incompatible with the set of inequalities equation (10), confirming that all three species need to be self-attracting for the eigenvalue to be complex. These predictions were again successfully verified by the results of our Brownian dynamics simulations.

5. Classification of generic cycles

5.1. Type-I instabilities in generic cycles

We now consider the general case with both nonzero substrate and product mobilities. In this more general case, networks can be built by choosing three of any of the six interaction patterns from figure 1(c), and there are then $6^3 = 216$ possible interaction networks. We show here that the presence or absence of certain motifs in the interaction network can be used to infer the stability of the full system by using a semi-diagrammatic approach. Similarly to cycles of product-insensitive species, we first calculate the non-null eigenvalues, which are found as

$$\lambda_{\pm} = -\frac{1}{2} \sum_{m=1}^{3} \Lambda_{m,m} \pm \frac{1}{2} \sqrt{\left(\sum_{m=1}^{3} \Lambda_{m,m} \right)^2 - 4 \sum_{m=1}^{3} \left(\Lambda_{m,m} \Lambda_{m+1,m+1} - \Lambda_{m+1,m} \Lambda_{m,m+1} \right)}. \tag{11}$$
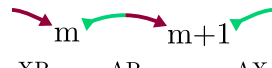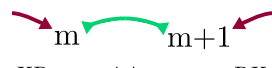
The homogeneous state is linearly unstable when the real part of the largest eigenvalue in equation (11) becomes positive, which leads to a type-I instability when

$$\sum_{m=1}^{3} \Lambda_{m,m} < 0, \tag{12}$$

effectively the same condition as equation (6), and corresponds to an overall self-attracting metabolic cycle.

Similarly to the case of product-insensitive species studied in section 4, any cycle of three self-attracting species is necessarily un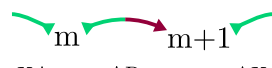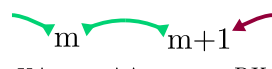stable according to equation (12). Cycles including at least one self-attracting and one self-repelling species can be either stable or unstable according to the type-I condition (table 1, first two lines). The presence of at least one self-attracting species is then sufficient to conclude on the possible stability behavior of a given cycle, independent of the rest of the interactions, which allows us to classify the 189 networks with at least one self-attracting species.

Table 2. Stability of all self-repelling pair motifs. Left column: exhaustive enumeration of pair interaction motifs composed of self-repelling species (labeled as 'Self R' in figure 1(c)). 'A' designates an attractive interaction, 'R' corresponds to a repulsive interaction, and 'X' can be any unspecified interaction. Middle column: condition on species mobilities for the corresponding term in equation (14) to be negative, i.e. instability-favoring. Right: contribution of the pair motif to the cycle stability, deduced from the corresponding middle-column condition (see appendix C for details). A species pair is written as stabilizing if the associated condition cannot be satisfied, destabilizing if it is always satisfied, and conditionally destabilizing if it the outcome depends on the mobility values.

Motif	Instability condition	Stability contribution
m $m+1$ XA RA RX	$\dfrac{\mu_{m+1}^{(s)}}{\mu_{m+1}^{(p)}} + \dfrac{\mu_m^{(p)}}{\mu_m^{(s)}} < 1$	Stabilizing
m $m+1$ XR AR AX	$\dfrac{\mu_{m+1}^{(s)}}{\mu_{m+1}^{(p)}} + \dfrac{\mu_m^{(p)}}{\mu_m^{(s)}} < 1$	Stabilizing
m $m+1$ XA AA AX	Trivially stable	Stabilizing
m $m+1$ XA RR XA	$\dfrac{\mu_{m+1}^{(s)}}{\mu_{m+1}^{(p)}} + \dfrac{\mu_m^{(p)}}{\mu_m^{(s)}} > 1$	Conditionally destabilizing
m $m+1$ XR AA RX	$\dfrac{\mu_{m+1}^{(s)}}{\mu_{m+1}^{(p)}} + \dfrac{\mu_m^{(p)}}{\mu_m^{(s)}} > 1$	Destabilizing
m $m+1$ XA AR AX	$\dfrac{\mu_{m+1}^{(p)}}{\mu_{m+1}^{(s)}}\left(1 - \dfrac{\mu_m^{(p)}}{\mu_m^{(s)}}\right) < 1$	Stabilizing
m $m+1$ XA AA RX	$\dfrac{\mu_{m+1}^{(p)}}{\mu_{m+1}^{(s)}}\left(1 - \dfrac{\mu_m^{(p)}}{\mu_m^{(s)}}\right) > 1$	Conditionally destabilizing
m $m+1$ XR AA AX	$\dfrac{\mu_m^{(s)}}{\mu_m^{(p)}}\left(1 - \dfrac{\mu_{m+1}^{(s)}}{\mu_{m+1}^{(p)}}\right) > 1$	Conditionally destabilizing
m $m+1$ XA RA AX	$\dfrac{\mu_m^{(s)}}{\mu_m^{(p)}}\left(1 - \dfrac{\mu_{m+1}^{(s)}}{\mu_{m+1}^{(p)}}\right) < 1$	Stabilizing

5.2. Stability of self-repelling species pairs

The 27 cycles that do not contain any self-attracting species can only exhibit a type-II instability, which corresponds to the following condition:

$$\sum_{m=1}^{3} \left(\Lambda_{m,m}\Lambda_{m+1,m+1} - \Lambda_{m,m+1}\Lambda_{m+1,m}\right) < 0. \tag{13}$$

This inequality involves the sum of three contributions, each of which corresponds to one of the three species pairs. We first determine which of the $3^2 = 9$ possible pairs of self-repelling species provide negative contributions to the sum written in equation (13) (see appendix C). To do so, we expand the terms of the sum as

$$\sum_{m=1}^{3} \alpha_m \alpha_{m+1} \Delta_{m,m+1} \rho_{0m}\rho_{0m+1} < 0, \tag{14}$$

using the following definition

$$\Delta_{m,m+1} = \tilde{\mu}_m^{(s)}\tilde{\mu}_{m+1}^{(s)} + \tilde{\mu}_m^{(p)}\tilde{\mu}_{m+1}^{(p)} - \tilde{\mu}_m^{(s)}\tilde{\mu}_{m+1}^{(p)}, \tag{15}$$

and find the conditions on the mobilities of each of the self-repelling species which leads to $\Delta_{m,m+1} < 0$ (see appendix C for the details of the derivation).

We compile the results in table 2. Out of the nine pairs of self-repelling species, five are always stabilizing, one is always destabilizing, and three are conditionally destabilizing, meaning that they favor instabilities if a certain inequality on the chemotactic mobilities of their constituent species is satisfied. Pairs that develop

chasing interactions are all stability-favoring, which can be predicted from equation (13) with all self-interactions $\Lambda_{m,m}$ positive. On the other hand, species pairs which favor instability all interact reciprocally and involve some degree of repulsion, which tends to make the pair more destabilizing when its magnitude is increased. This is exemplified by the fact that the only pair which is always instability-favoring, whose interactions can be described as XR–AA–RX, involves two species which reciprocally attract and are repelled by their other neighbor.

5.3. Stability of cycles of self-repelling species

Using the information gathered on the pairs of self-repelling species, we systematically classify the remaining 27 networks of only self-repelling species. We further reduce that number to seven 'elementary' networks onto which any cycle of self-repelling species can be mapped through symmetry operations, using the invariance of the eigenvalue equation (11) under cyclic swap of the catalytic species, and the invariance of equation (13) under mirror symmetry around one pair (see appendix D). We then classify the stability of each elementary network based on which species pair they contain.

We find that two networks contain the always destabilizing pair XR–AA–RX table 2, and are thus unstable if the magnitude of the activities, mobilities, or homogeneous concentrations associated to it are tuned so that the associated term in equation (13) overcomes the stabilizing term from the other pairs. As these cycles can be made unstable simply by adjusting the parameters in order to give enough weight to one-pair terms, we call them type-IIa, or strongly, unstable. Another cycle, whose pair interactions go as AA–AA–RR, contains three conditionally destabilizing pairs. However, the inequalities to be satisfied for all three pairs to be stable are incompatible, and at least one of the three is necessarily instability-favoring. This cycle can then also be classified as type-IIa-unstable, with the only difference with the two previous one being that the instability-favoring pair can be different based on the choice of mobilities.

Two more elementary cycles can be made unstable, but with stricter criteria than those of type-IIa. These cycles only contain species pairs which are either stabilizing, or conditionally destabilizing. In order for these to be unstable, two criteria then need to be fulfilled: the species mobilities must be chosen so that at least one conditionally destabilizing pair is unstable, and enough weight must be given in equation (13) to this pair, so that the whole cycle is unstable, a condition which we name type-IIb (or weakly) unstable networks. Finally, two elementary cycles are only composed of stabilizing pairs, and thus cannot be made unstable.

6. Discussion

In this work, we have studied the behavior of a metabolic cycle of three catalytic species which chemotax in response to gradients of their substrates and products, and interact nonreciprocally owing to these two properties. We have demonstrated that the interaction network between the species can be built by independently choosing one interaction pattern per species, and that the stability of the resulting network can be determined by independently considering single-species and species-pair motifs. For the particular case of cycles composed of species with no chemotaxis in response to product gradients (only in response to substrate gradients), we have calculated a parameter-free stability line and used it to classify all the possible interaction networks in such cycles. We found that, for this reduced model, at least one self-attracting interaction motif must be present in order to observe self-organization. For cycles of species chemotactic in response to both substrate and product gradients, we derived two instability criteria from which the stability behavior of any choice of interaction motifs can be determined. The first condition (type-I) concerns the single-species interaction motifs, and translates the fact that the presence of a self-attracting species is sufficient for a cycle to potentially be unstable. In the case in which a cycle is composed strictly of self-repelling species, a second condition (type-II) becomes relevant, which involves interaction motifs between pairs of species. The contribution to all possible pair interaction motifs to this condition can be classified as either stabilizing, destabilizing, or conditionally destabilizing. In turn, this classification of pairs can be used to classify the stability of self-repelling cycles according to the pair motifs that they contain, and distinguish type-II unstable cycles as type-IIa, or strongly, unstable if they contain at least a destabilizing species pair, and type-IIb, or weakly, unstable if they only contain conditionally destabilizing (and stabilizing) pairs.

We have restricted our investigation here to size-three metabolic cycles, which are structures of small size and complexity compared to many biologically-relevant metabolic pathways. An immediate extension would then be to use the methods we developed for small cycles and to apply them to larger chemical reaction networks, or to non-cycle geometries. The most straightforward generalization is the study of metabolic cycles of more than three species, which have already been shown to exhibit complex and cycle-size-dependent behavior [18]. Intriguingly, our motif-based classification has shown that, in a size-three cycle, pair interactions can lead to self-organization with more relaxed conditions than non-cyclic

topologies. In particular, self-organization may occur even for systems in which all species are self-repelling, as studied in more detail in [17]. Larger cycle sizes likely result in the emergence of higher-order terms in the linear stability analysis (for instance, triplets of species in a size-four cycle), which could further relax the instability condition and lead to new types of instability. In the context of larger, more complex biochemical reaction networks, one possible approach could be to identify and analyze small key motifs in the reaction pathway, akin to the network motifs which are studied in systems biology [39, 40] and other disciplines [41].

Ultimately, our work shows that there is a spontaneous, emergent route for the spatial self-organization of catalysts that participate in a common metabolic pathway. This provides an alternative route for the formation of enzyme-rich clusters in cells, also known as *metabolons* [42, 43], not relying on scaffolding proteins or lock-and-key, direct enzyme-enzyme interactions. Recent works have demonstrated that the spatial self-organization of enzymes (in this case assumed by construction, rather than emergent) can optimize the overall reaction rate of a pathway [44] or be used as a method for regulating the output of a branch in a reaction network [45]. Conversely, the spatial arrangement of catalysts can be designed to increase reaction yield [46], implying that reaction networks could be also be designed with a similar goal in mind by choosing catalysts which self-organize into a reaction-flux-optimizing structure. Such effects could be investigated in the context of our model metabolic cycles, for instance by particularizing one of the reaction products and studying the effect of self-organization on its production rate. The overall metabolic fluxes of the now emergent, self-organized structure will then depend on the motifs present in the underlying network of effective interactions. Finally, we note that such non-reciprocal interactions can be used to design shape-shifting self-organized complexes reminiscent of structures that appear during the different phases of the cell cycle [47].

Data availability statement

All data that support the findings of this study are included within the article (and any supplementary files).

Acknowledgments

Appendix A. Linear stability analysis

The stability of a size-three metabolic cycle can be determined by performing a linear stability analysis of equations (1) and (2) as follows. We consider a homogeneous steady state of equations (1) and (2), with time- and space-independent concentrations c_{0k} for chemical species k and ρ_{0m} for catalytic species m. We then perturb this steady state with perturbations $\delta\rho_n(\mathbf{r}, t)$ and $\delta c_k(\mathbf{r}, t)$, and develop equations (1) and (2) to the first order in perturbation. With the quasi-steady-state assumption that $\partial_t \delta c_k = 0$, corresponding to the limit of fast-diffusing chemicals species, and using the Fourier mode decomposition $\delta\rho_n = \delta\rho_n(\mathbf{k})e^{\lambda t}e^{i\mathbf{k}\mathbf{r}}$ and $\delta c_k = \delta c_k(\mathbf{k})e^{\lambda t}e^{i\mathbf{k}\mathbf{r}}$, we obtain the following equation:

$$\left(\lambda + D_p k^2\right)\delta\rho_m(\mathbf{k}) = -\sum_{n=1}^{3}\Lambda_{m,n}\delta\rho_n(\mathbf{k}). \tag{A1}$$

It is easily seen that, if $\text{Re}(\lambda) > 0$, then the $k = 0$ mode, which corresponds to a system-wide perturbation, is the most unstable one. We then focus our analysis on that mode, and to simplify notation use $\delta\rho_m \equiv \delta\rho_m(k = 0)$, which leads to equation (3).

Appendix B. Brownian dynamics simulation

In order to test the stability criteria for strictly substrate-chemotactic species given in equations (8) and (10), we perform Brownian dynamics simulations of our system. We consider spherical catalysts of diameter σ, which we also take as the size scale for our simulations, and assume that they isotropically convert their substrate into their product on their surface at a rate α.

We first derive the expression for the velocity which a catalytically-active particle develops as a response to the presence of another particle. Using the same quasi-steady state approximation used in the linear

stability analysis, we can write that the concentration field associated with species k follows at any time the Laplace equation

$$D^{(k)} \nabla^2 c_k = 0, \tag{B1}$$

with boundary conditions obtained by balancing the reactive and diffusive fluxes at the surface of the catalysts. A particle with index i induces a velocity response for another particle j by creating perturbations of the latter's substrate and product concentrations, which we write as $\delta c^{s(j)}$ and $\delta c^{p(j)}$ respectively. The corresponding velocity of j in the presence of i is then $\boldsymbol{v}_{ji} = \boldsymbol{v}_{ji}^{s} + \boldsymbol{v}_{ji}^{p}$ with $\boldsymbol{v}_{ji}^{s} = -\mu_j^{(s)} \nabla \delta c_i^{s(j)}$ and $\boldsymbol{v}_{ji}^{p} = -\mu_j^{(s)} \nabla \delta c_i^{p(j)}$, which finally results in:

$$\boldsymbol{v}_{ji} = \frac{\Lambda_{j,i}}{4\pi} \frac{\boldsymbol{r}_{ji}}{r_{ji}^3} \tag{B2}$$

where $\boldsymbol{r}_{ji} = \boldsymbol{r}_j - \boldsymbol{r}_i$, and Λ is defined as in (4) except without the density ρ_{0m}.

The location $\boldsymbol{r}_i$ of catalyst i then evolves according to the Langevin equation

$$\frac{\mathrm{d}}{\mathrm{d}t} \boldsymbol{r}_i(t) = \sum_{j \neq i} \boldsymbol{v}_{ij} + \sqrt{2D_p} \boldsymbol{\eta}_i \tag{B3}$$

where $\boldsymbol{\eta}_i$ is a centered Gaussian white noise with intensity one. We simulate a mixture of three species, each of which has a population N_m, yielding a set of $N_1 + N_2 + N_3$ Langevin Equations which we integrate using the forward Euler method with time step $\mathrm{d}t$ for a duration t_{tot}. The three chemical species are assumed to have the same diffusion coefficient, $D^{(1)} = D^{(2)} = D^{(3)} = D$. The quantities α_0 and μ_0 are arbitrary activity and mobility scales, from which a time scale $\tau = \alpha_0 \mu_0 / (4\pi D \sigma^3)$ and a diffusion coefficient scale $D_0 = (4\pi \sigma) / \alpha_0 \mu_0$ can be built. The particles are simulated in a cubic box of size chosen so that the particles occupy a volume fraction $\Phi = 0.005$, with the interactions implemented according to the minimum image convention. Finally, we simulate short-range repulsion between the catalytic particles by performing an overlap correction after each time step using the elastic collision method described in [48].

To generate the phase diagram shown in figure 2, we simulate a set of $N_1 = N_2 = N_3 = 500$ particles with the following parameters: activity $\alpha/\alpha_0 = 1$, time step $\mathrm{d}t/\tau = 0.001$, simulation duration $t_{tot}/\tau = 600$, noise intensity $D_p/D_0 = 0.01$. The mobility of species 1 is fixed at $\mu_1^{(s)}/\mu_0 = \pm 0.33$, and the mobilities of species 2 and 3 are taken on a 20 by 20 grid with range $\mu_{2,3}^{(s)}/\mu_0 \in [-3, 3]$.

Appendix C. Determination of pair instability conditions

We use the fact that the three possible interaction motifs for self-repelling species are each associated to certain constraints on the species mobilities (see figure 1(c) for the mobility signs corresponding to the interactions):

- XA–RX: As $\mu_m^{(s)} < 0, \mu_m^{(p)} < 0, \mu_m^{(p)} > \mu_m^{(s)}$, we can write:

$$0 < \frac{\mu_m^{(p)}}{\mu_m^{(s)}} < 1. \tag{C1}$$
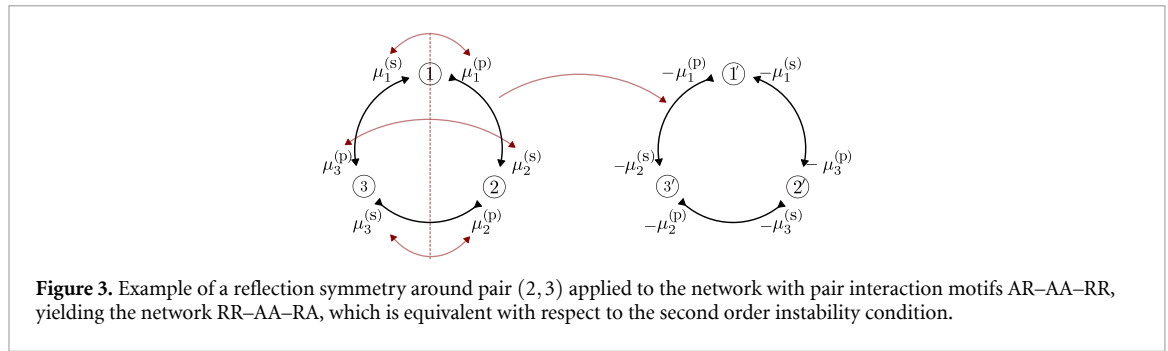
- XR–AX: As $\mu_m^{(s)} > 0, \mu_m^{(p)} > 0, \mu_m^{(p)} > \mu_m^{(s)}$, we can write:

$$0 < \frac{\mu_m^{(s)}}{\mu_m^{(p)}} < 1. \tag{C2}$$

- XA–AX: As $\mu_m^{(s)} < 0, \mu_m^{(p)} > 0$, we can write:

$$\frac{\mu_m^{(p)}}{\mu_m^{(s)}} < 0. \tag{C3}$$

We then study the stability of all possible pairs of these motifs. To do so, we first write the pair stability factor as given by equation (13). We write the condition $\Delta_{m,m+1} < 0$, subtract the negative terms so that the inequality only involves positive quantities, and rewrite the resulting inequality into a condition involving the ratios $\frac{\mu_{m \text{ or } m+1}^{(s)}}{\mu_{m \text{ or } m+1}^{(p)}}$ and $\frac{\mu_{m \text{ or } m+1}^{(p)}}{\mu_{m \text{ or } m+1}^{(s)}}$. From the conditions in equations (C1)–(C3), it can then be determined whether

Figure 3. Example of a reflection symmetry around pair $(2, 3)$ applied to the network with pair interaction motifs AR–AA–RR, yielding the network RR–AA–RA, which is equivalent with respect to the second order instability condition.

the motif is unstable. For instance, for the interaction motif XA–RA–RX, the condition can be rearranged to have positive left- and right-hand-side terms as $\mu_m^{(p)}\mu_{m+1}^{(p)} + \mu_m^{(s)}\mu_{m+1}^{(s)} < \mu_m^{(s)}\mu_{m+1}^{(p)}$. This inequality can be further rearranged in terms of mobility ratios under the previously enumerated constraints as $\frac{\mu_{m+1}^{(s)}}{\mu_{m+1}^{(p)}} + \frac{\mu_m^{(p)}}{\mu_m^{(s)}} < 1$. Because $\frac{\mu_{m+1}^{(s)}}{\mu_{m+1}^{(p)}} > 1$ and $\frac{\mu_m^{(p)}}{\mu_m^{(s)}} > 0$, this condition is impossible to realize: the motif is always stable. By systematically applying this recipe, we analyze the stability of all motifs, which is given in table 2.

Appendix D. Mirror symmetry operation

One key aspect making the classification of cyclic networks easier is that the stability conditions are invariant under reflection symmetry around a pair of species. The corresponding symmetry operation is to swap the interaction network around a reflection line. For instance, applying a reflection symmetry around pair $(2,3)$ involves:

- Turning $\mu_1^{(s)}$ into $-\mu_1^{(p)}$ and vice versa
- Turning $\mu_2^{(p)}$ into $-\mu_3^{(s)}$ and vice versa
- Turning $\mu_2^{(s)}$ into $-\mu_3^{(p)}$ and vice versa

with the sign change of the mobilities coming from the fact that substrate and product interactions of the same signs have opposite associated mobility signs. See figure 3 for a graphical example. Additionally, the activities and homogeneous densities of the species whose mobilities are swapped also need to be exchanged.

The stability of all possible networks of self-repelling species can then be determined by enumerating them and, for a given network, applying the cyclic swap and reflection symmetry to determine all equivalent networks. We can group the interaction networks of self-repelling species into three classes, based on whether they contain one, two, or three unique motifs. We determine the stability of each of the retained elementary networks using the method described in section 5.2, and compile the results in table 1.

ORCID iDs

Vincent Ouazan-Reboul ⬤ https://orcid.org/0009-0002-7720-8881
Ramin Golestanian ⬤ https://orcid.org/0000-0002-3149-4002
Jaime Agudo-Canalejo ⬤ https://orcid.org/0000-0001-9677-6054

References

[1] Golestanian R 2022 Phoretic active matter *Active Matter and Nonequilibrium Statistical Physics (Lecture Notes of the Les Houches Summer School* vol 112*)* (Oxford University Press)
[2] Varma A, Montenegro-Johnson T D and Michelin S 2018 Clustering-induced self-propulsion of isotropic autophoretic particles *Soft Matter* **14** 7155
[3] Stark H 2018 Artificial chemotaxis of self-phoretic active colloids: collective behavior *Acc. Chem. Res.* **51** 2681
[4] Saha S, Golestanian R and Ramaswamy S 2014 Clusters, asters and collective oscillations in chemotactic colloids *Phys. Rev.* E **89** 062316
[5] Schmidt F, Liebchen B, Löwen H and Volpe G 2019 Light-controlled assembly of active colloidal molecules *J. Chem. Phys.* **150** 094905
[6] Golestanian R 2012 Collective behavior of thermally active colloids *Phys. Rev. Lett.* **108** 038303
[7] Cohen J A and Golestanian R 2014 Emergent cometlike swarming of optically driven thermally active colloids *Phys. Rev. Lett.* **112** 068302
[8] Keller E F and Segel L A 1970 Initiation of slime mold aggregation viewed as an instability *J. Theor. Biol.* **26** 399
[9] Gelimson A and Golestanian R 2015 Collective dynamics of dividing chemotactic cells *Phys. Rev. Lett.* **114** 028101

[10] Soto R and Golestanian R 2014 Self-assembly of catalytically active colloidal molecules:tailoring activity through surface chemistry *Phys. Rev. Lett.* **112** 068301

[11] Soto R and Golestanian R 2015 Self-assembly of active colloidal molecules with dynamic function *Phys. Rev. E* **91** 052304

[12] Sengupta A, Kruppa T and Löwen H 2011 Chemotactic predator-prey dynamics *Phys. Rev. E* **83** 031914

[13] Meredith C H, Moerman P G, Groenewold J, Chiu Y-J, Kegel W K, van Blaaderen A and Zarzar L D 2020 Predator–prey interactions between droplets driven by non-reciprocal oil exchange *Nat. Chem.* **12** 1136

[14] Saha S, Agudo-Canalejo J and Golestanian R 2020 Scalar active mixtures: the nonreciprocal Cahn-Hilliard model *Phys. Rev. X* **10** 041009

[15] Fruchart M, Hanai R, Littlewood P B and Vitelli V 2021 Non-reciprocal phase transitions *Nature* **592** 363

[16] Agudo-Canalejo J and Golestanian R 2019 Active phase separation in mixtures of chemically interacting particles *Phys. Rev. Lett.* **123** 018101

[17] Ouazan-Reboul V, Golestanian R and Agudo-Canalejo J 2023 Network effects lead to self-organization in metabolic cycles of self-repelling catalysts *Phys. Rev. Lett.* **131** 128301

[18] Ouazan-Reboul V, Agudo-Canalejo J and Golestanian R 2023 Self-organization of primitive metabolic cycles due to non-reciprocal interactions *Nat. Commun.* **14** 4496

[19] Dill K A, Ozkan S B, Shell M S and Weikl T R 2008 The protein folding problem *Annu. Rev. Biophys.* **37** 289

[20] Dill K A 1985 Theory for the folding and stability of globular proteins *Biochemistry* **24** 1501

[21] Phillips R, Kondev J, Theriot J, Garcia H G and Orme N 2012 *Physical Biology of the Cell* 2nd edn (Garland Science)

[22] Hoque T, Chetty M and Sattar A 2009 Extended HP model for protein structure prediction *J. Comput. Biol.* **16** 85

[23] Chan H S 1999 Folding alphabets *Nat. Struct. Biol.* **6** 994

[24] Riddle D S, Santiago J V, Bray-Hall S T, Doshi N, Grantcharova V P, Yi Q and Baker D 1997 Functional rapidly folding proteins from simplified amino acid sequences *Nat. Struct. Biol.* **4** 805

[25] Jumper J *et al* 2021 Highly accurate protein structure prediction with alpha fold *Nature* **596** 583

[26] Li H, Helling R, Tang C and Wingreen N 1996 Emergence of preferred structures in a simple model of protein folding *Science* **273** 666

[27] Li H, Tang C and Wingreen N S 1998 Are protein folds atypical? *Proc. Natl Acad. Sci.* **95** 4987

[28] Lim W A and Sauer R T 1989 Alternative packing arrangements in the hydrophobic core of λ repressor *Nature* **339** 31

[29] Kamtekar S, Schiffer J M, Xiong H, Babik J M and Hecht M H 1993 Protein design by binary patterning of polar and nonpolar amino acids *Science* **262** 1680

[30] Antoniewicz M R 2015 Methods and advances in metabolic flux analysis: a mini-review *J. Indus. Microbiol. Biotechnol.* **42** 317

[31] Orth J D, Thiele I and Palsson B Ø 2010 What is flux balance analysis? *Nat. Biotechnol.* **28** 245

[32] Visser D and Heijnen J J 2002 The mathematics of metabolic control analysis revisited *Metabol. Eng.* **4** 114

[33] Erklavec Zajec V, Novak U, Kastelic M, Japelj B, Lah L, Pohar A and Likozar B 2021 Dynamic multiscale metabolic network modeling of chinese hamster ovary cell metabolism integrating n-linked glycosylation in industrial biopharmaceutical manufacturing *Biotechnol. Bioeng.* **118** 397

[34] Ouazan-Reboul V, Agudo-Canalejo J and Golestanian R 2021 Non-equilibrium phase separation in mixtures of catalytically active particles: size dispersity and screening effects *Eur. Phys. J. E* **44** 113

[35] Jee A-Y, Dutta S, Cho Y-K, Tlusty T and Granick S 2018 Enzyme leaps fuel antichemotaxis *Proc. Natl Acad. Sci.* **115** 14–18

[36] Agudo-Canalejo J, Adeleke-Larodo T, Illien P and Golestanian R 2018 Enhanced diffusion and chemotaxis at the nanoscale *Acc. Chem. Res.* **51** 2365

[37] Feng M and Gilson M K 2020 Enhanced diffusion and chemotaxis of enzymes *Annu. Rev. Biophys.* **49** 87

[38] Zhao X, Palacci H, Yadav V, Spiering M M, Gilson M K, Butler P J, Hess H, Benkovic S J and Sen A 2018 Substrate-driven chemotactic assembly in an enzyme cascade *Nat. Chem.* **10** 311

[39] Alon U 2007 Network motifs: theory and experimental approaches *Nat. Rev. Genet.* **8** 450

[40] Milo R, Shen-Orr S, Itzkovitz S, Alon U, Alon U and Alon U 2002 Network motifs: simple building blocks of complex networks *Science* **298** 824 2002

[41] Stone L, Simberloff D and Artzy-Randrup Y 2019 Network motifs and their origins *PLOS Comput. Biol.* **15** e1006749

[42] Wu F, Pelster L N and Minteer S D 2015 Krebs cycle metabolon formation: metabolite concentration gradient enhanced compartmentation of sequential enzymes *Chem. Commun.* **51** 1244

[43] Sweetlove L J and Fernie A R 2018 The role of dynamic enzyme assemblies and substrate channelling in metabolic regulation *Nat. Commun.* **9** 2136

[44] Buchner A, Tostevin F and Gerland U 2013 Clustering and optimal arrangement of enzymes in reaction-diffusion systems *Phys. Rev. Lett.* **110** 208104

[45] Hinzpeter F, Tostevin F and Gerland U 2019 Regulation of reaction fluxes via enzyme sequestration and co-clustering *J. R. Soc. Interface* **16** 20190444

[46] Xie C, Chen C, Yu Y, Su J, Li Y, Somorjai G A and Yang P 2017 Tandem catalysis for CO2 hydrogenation to C2–C4 hydrocarbons *Nano Lett.* **17** 3798

[47] Osat S and Golestanian R 2022 Non-reciprocal multifarious self-organization *Nat. Nanotechnol.* **18** 79

[48] Strating P 1999 Brownian dynamics simulation of a hard-sphere suspension *Phys. Rev. E* **59** 2175